Liquid Crystals
Publication details, including instructions for authors and subscription information:
http://www.informaworld.com/smpp/title~content=t713926090

Antiferroelectric and ferrielectric liquid crystalline low molar mass materials and polymers

S. Mery; D. Lotzsch; G. Heppke; R. Shashidhar

Online publication date: 29 June 2010

To cite this Article Mery, S. , Lotzsch, D. , Heppke, G. and Shashidhar, R.(1997) 'Antiferroelectric and ferrielectric liquid crystalline low molar mass materials and polymers', Liquid Crystals, 23: 5, 629 — 644
To link to this Article: DOI: 10.1080/026782997207902
URL: http://dx.doi.org/10.1080/026782997207902

LIQUID CRYSTALS, 1997, VOL. 23, NO. 5, 629–644

Antiferroelectric and ferrielectric liquid crystalline low molar mass materials and polymers

by S. MERY*, D. LOTZSCH†, G. HEPPKE† and R. SHASHIDHAR

Center for Bio/Molecular Science and Engineering, Naval Research Laboratory, Washington DC 20375-5348, USA

†Technische Universität Berlin, Strasse des 17 Juni 135, 10623 Berlin, Germany

(*Received 10 March 1997; in final form 1 May 1997; accepted 12 June 1997*)

Novel liquid crystalline Low Molecular Mass (LMM) materials bearing two chiral lactate groups, as well as compounds of like structure to **MHPOBC** have been synthesized. All the LMM compounds exhibit the SmC_A^* (antiferroelectric) and/or SmC_γ^* (ferrielectric) phases. The mesogens have been incorporated as pendant groups on polymer backbones of three different natures to prepare side chain liquid crystalline copolysiloxanes, homopolysiloxanes and homopolyacrylates. The investigation of the polymers by means of miscibility studies showed that the antiferro- and ferri-electric phases are strongly destabilized in the coposiloxanes and homopolysiloxanes, while in the homopolyacrylates a large temperature range mesophase is found to be miscible with the SmC_A^* phase. The physical properties of the mesophases and their stability, both for the LMM materials and the polymers, are presented and discussed.

1. Introduction

In recent years, chirality in liquid crystals has become a topic of high interest. Among the new chiral mesophases are the antiferroelectric and ferrielectric smectic phases in which interest extends from theoretical aspects to technical applications [1].

In the antiferroelectric smectic C* phase (denoted SmC_A^* [2] or SmO* [3, 4]; these two phases, found independently in different compounds, are miscible and so should be regarded as identical [5, 6]), the tilt direction of the molecules alternates from layer to layer, so that the polarization vectors point out in opposite directions in successive layers [7, 8]. The structure of the ferrielectric smectic C* phase (SmC_γ^*) is thought to be made up from periodically repeated blocks of ferroelectric and antiferroelectric ordering [9–11]. Because of the chirality, a helical macrostructure with the helical axis along the layer normal appears in an unperturbed condition. The general structures of the ferroelectric and antiferroelectric smectic phases in the unwound states are depicted in figure 1. Under an electric field, the antiferroelectric and ferrielectric mesophases can reveal a tristable [12] and tetrastable [13] switching, respectively, giving rise to potential applications in liquid crystal displays [1]. In spite of the large amount of work devoted to the antiferro- and ferri-electric mesophases, the molecular origin of the formation of these mesophases has not been clearly elucidated as yet. However, some authors have suggested that the SmC_A^* phase might be stabilized by the pairing energy of transverse dipole moments in adjacent smectic layers, while for the SmC* phase, it should be stabilized by a packing energy effect resulting from the temperature-dependent excluded volume effect [1, 14, 15]. Also, there was observed a higher smectic order parameter in the SmC_A^* than in the SmC* phase, revealing a better lateral register of the

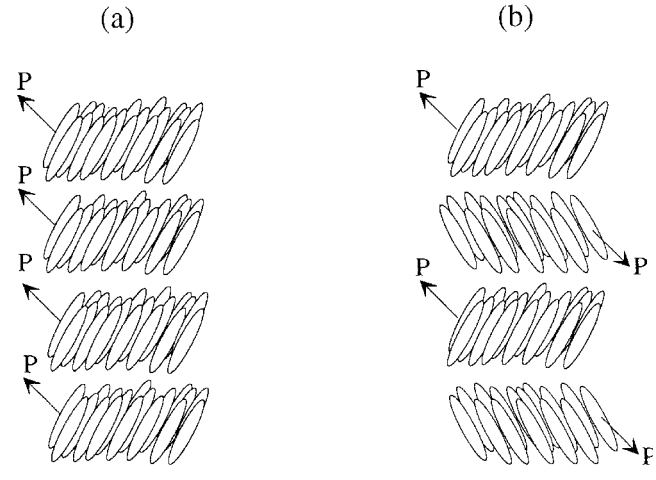

Figure 1. Molecular ordering of the ferroelectric (*a*) and the antiferroelectric (*b*) smectic phases in the unwound state.

*Author for correspondence.

*Current address: IPCMS/Groupe des Matériaux Organiques, 23 rue du Loess, BP20 CR, F-67037 Strasbourg Cedex Fax +33 31 8 8 10 72 46.

molecules within the layers in the antiferroelectric phase [1, 16]. On the other hand, it has been mentioned that the SmC^*_γ phase would appear as a result of competition between the two driving forces stabilizing the SmC^*_A and SmC* phases [1, 15].

To date, a large number of antiferroelectric liquid crystals have been reported. However, the materials are essentially low molecular mass systems and generally correspond to a few kinds of molecular structures. Among them are 4-(1-methylheptyloxycarbonyl)phenyl 4′-octyloxybiphenyl-4-carboxylate (**MHPOBC**) [12] and its numerous derivatives. A few antiferroelectric liquid crystal materials exhibit additional sub-phases, such as the SmC^*_γ phase [1]. In most cases, no significant variation in the molecular structure has been made on the chiral part, which generally contains only one asymmetric centre. More often, the chiral part is composed of a ramified hydrocarbon or fluorohydrocarbon chain, connected to the rigid aromatic core by an ester or a ketone group.

With regard to chiral polymeric materials, very few investigations have been performed in that field, so far. Indeed, the characterization of antiferroelectricity in polymers is generally quite difficult, particularly because of the high melt viscosity of the materials. However, a handful of liquid crystalline polymers has been reported (probably) to show an antiferroelectric ordering [17–24], but only some of them could clearly exhibit antiferroelectric behaviour (i.e. a third switching state) [19–22]. Except in the case of a series of main chain polymers [23], all of the materials are side group liquid crystalline polymers and have the peculiarity of having a polyacrylate backbone. It must be mentioned that a recent publication of Nishiyama and Goodby reported antiferroelectric polyacrylates in which the SmC^*_A phase was found to be strongly stabilized upon polymerization [22]. These authors suggested the stabilization of the antiferroelectric phase in the polymers might result from dipole–dipole interaction effects and/or from a conformational effect of the polymer backbone. Finally, on the single basis of small angle X-ray investigations, a mesophase with a 'ferrielectric character' was assumed to be present in a series of combined liquid crystalline polymers [24].

Chirality is not a prerequisite for the formation of a smectic phase with zig-zag ordering. Firstly, a herringbone structure was identified in several racemic mixtures of antiferroelectric compounds [8, 25–27], as well as in a series of pure non-chiral liquid crystal materials [28–30]. Secondly, non-chiral main chain liquid crystalline polyesters were found to exhibit a smectic phase with a zig-zag structure (SmC_2) or a normal SmA phase, depending on the number of the methylene units in the spacer [31, 32]. Similar behaviour was observed with dimeric model compounds of these polymers, for which the appearance of these phases could be related to the *trans*-conformational order of the spacer chain [33]. It must be noted that the SmC_2 phase of one such dimer has been shown not to be miscible with the SmC^*_A or SmO* phase [6]. Unlike the antiferroelectric phase, the ferrielectric smectic phase (SmC^*_γ) is found to be greatly dependent on the optical purity of the compounds [25, 27, 34], and to our knowledge no ferrielectric-like mesophase has been observed in non-chiral liquid crystal materials.

In order to help reach an understanding of the stability of the antiferroelectric and ferrielectric mesophases in liquid crystalline materials, we have synthesized the two series of LMM compounds and the three series of polymers presented in figures 2 and 3, respectively. The first series of LMM materials are liquid crystals structurally close to **MHPOBC** (**M1a**, **M1b**); the second series are mesogens for which the rigid core is the same as **MHPOBC**, but having a strongly polar chiral moiety composed of two chiral lactate groups (**M2**, **M2a**, **M2b**). As starting materials for the preparation of the side group liquid crystalline polysiloxanes and polyacrylates, these mesogens bear a vinylic (**M1a**, **M2a**) or an acrylate (**M1b**, **M2b**) end group on their peripheral alkyl chain. The chemical structure of the polymers is presented in figure 3. Three different kinds of polymeric backbones have been investigated: a copolysiloxane backbone for which about 30% of the siloxane units are connected to a mesogenic side group (**CPS1**, **CPS2**), a homopolysiloxane (**HPS1**, **HPS2**) and a homopolyacrylate (**HPA1**, **HPA2**) backbone. This paper reports and discusses the stability of the antiferroelectric and ferrielectric mesophases, both in the LMM materials and the polymers, as a function of the chemical structures of the materials, and as a function of the nature of the polymer backbone.

2. Synthetic part

2.1. *Preparation of the materials*

The low molecular mass materials were synthesized by using classical reactions, already described in the literature [35]. The synthetic procedure for the preparation of the polymers, as well as the chemical characterization data for all materials are reported below.

(S)-4-(1-methylheptyloxycarbonyl)phenyl 4′-(9-decenyloxy)biphenyl-4-carboxylate (**M1a**). Elemental analysis: calculated (found) for $C_{38}H_{48}O_5$: C 78·05(77·99), H 8·27(8·29). ^{1}H NMR ($CDCl_3$, TMS) δ (ppm): 0·9 (t, 3H, CH_3), 1·25–1·8 (m, 25H, CH_2 and CH*–C$\underline{H}_3$), 2·05 (m, 2H, C$\underline{H}_2$–CH–CH_2), 4·0 (t, 2H, CH_2O), 5·0 (m, 2H, CH–C$\underline{H}_2$), 5·15 (m, 1H, C$\underline{H}$*), 5·8 (m, 1H, C$\underline{H}$–CH_2), 7·0–8·25 (12H, ArH).

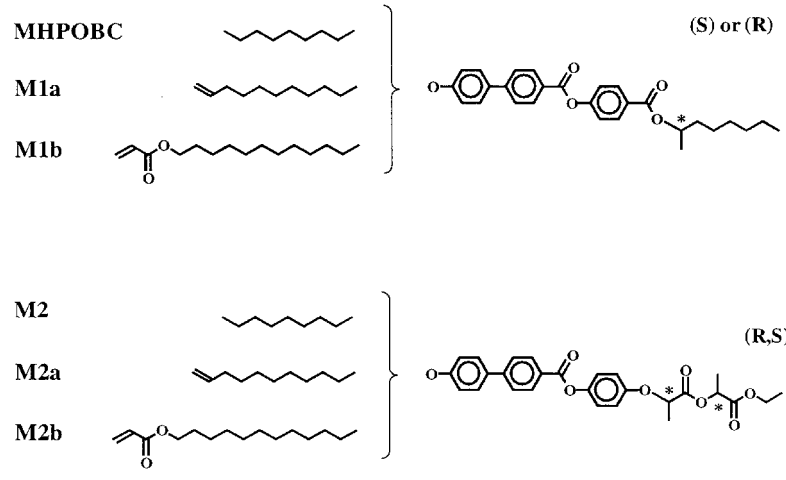

Figure 2. Chemical structures of the two series of antiferroelectric and ferrielectric low molecular mass materials.

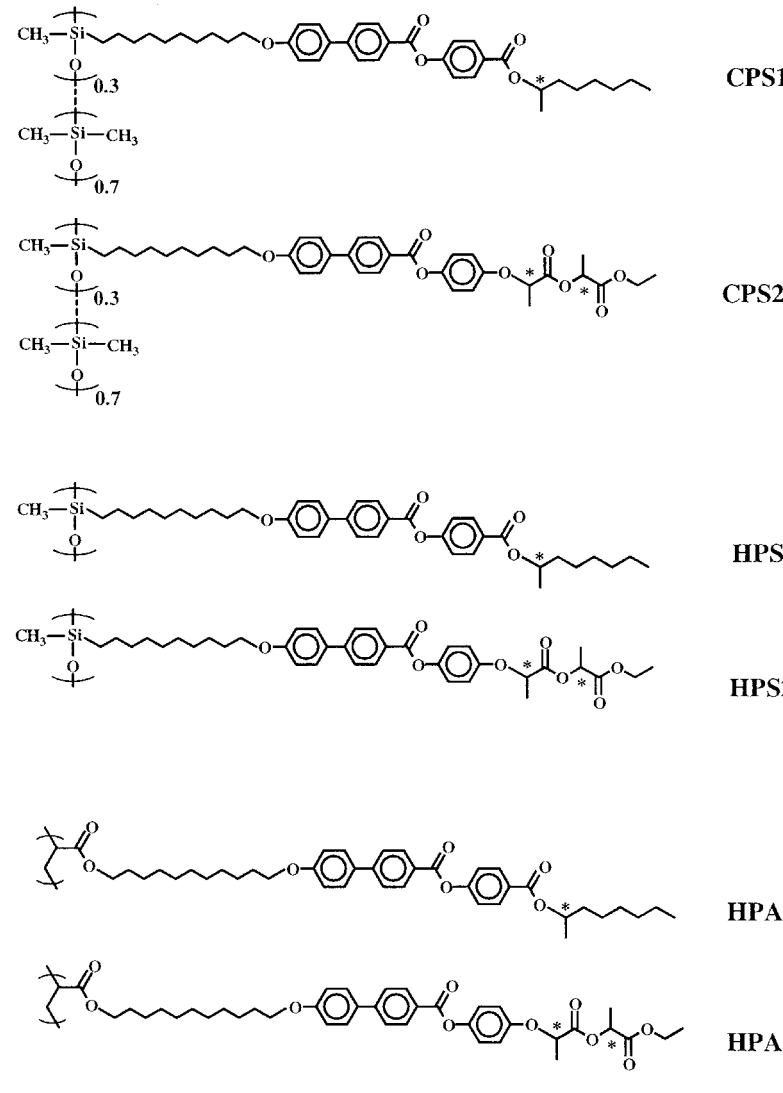

Figure 3. Chemical structures of the side group liquid crystalline copolysiloxanes (**CPS1**, **CPS2**), homopolysiloxanes (**HPS1**, **HPS2**) and homopolyacrylates (**HPA1**, **HPA2**).

(S)-4-(1-methylheptyloxycarbonyl)phenyl 4′-(11-propenoyloxyundecanoxy)biphenyl-4-carboxylate (**M1b**). Elemental analysis: calculated(found) for $C_{42}H_{54}O_7$: C 75·19(75·13), H 8·11(8·13). ^{1}H NMR ($CDCl_3$, TMS) δ (ppm): 0·9 (t, 3H, CH_3), 1·25–1·8 (m, 31H, CH_2 and CH*–C$\underline{H}_3$), 4·0 (t, 2H, CH_2OAr), 4·15 (t, 2H, $COOCH_2$), 5·15 (m, 1H, C$\underline{H}$*), 5·8 and 6·4 (m, 2H, CH=C$\underline{H}_2$), 6·1 (m, 1H, C$\underline{H}$=CH_2), 7·0–8·25 (12H, ArH).

1-(R)-[1-(S)-ethoxycarbonyl)ethoxycarbonyl]ethoxyphenyl 4′-octyloxybiphenyl-4-carboxylate (**M2**). Elemental analysis: calculated(found) for $C_{35}H_{42}O_8$: C 71·16(71·32), H 7·17(7·20), O 21·67(21·51). ^{1}H NMR ($CDCl_3$, TMS) δ (ppm): 0·9 (t, 3H, CH_3), 1·25–1·45 (m, 13H, $COOCH_2$–C$\underline{H}_3$, CH_2), 1·5 (d, 3H, ArOCH*–C$\underline{H}_3$), 1·7 (d, 3H, C$\underline{H}_3$–CH*–$COOCH_2$), 1·8 (m, 2H, C$\underline{H}_2$–CH_2O), 4·0 (t, 2H, $ArOCH_2$), 4·2 (q, 2H, $COOCH_2$), 4·8 (q, 1H, ArOCH*), 5·15 (q, 1H, C$\underline{H}$*$COOCH_2$), 7·0–8·2 (12H, ArH).

1-(R)-[1-(S)-ethoxycarbonyl)ethoxycarbonyl]ethoxyphenyl 4′-(9-decanyloxy)biphenyl-4-carboxylate (**M2a**). Elemental analysis: calculated(found) for $C_{37}H_{44}O_8$: C 72·06(71·85), H 7·19(7·20). ^{1}H NMR ($CDCl_3$, TMS) δ (ppm): 1·25 (t, 3H, OCH_2–C$\underline{H}_3$), 1·3–2·05 (m, 20H, CH_2 and CH*–C$\underline{H}_3$), 4·0 (t, 2H, $ArOCH_2$), 4·2 (q, 2H, $COOCH_2$), 4·85 (q, 1H, ArOCH*), 5·0 (m, 2H, CH=C$\underline{H}_2$), 5·15 (q, 1H, C$\underline{H}$*$COOCH_2$), 5·85 (m, C$\underline{H}$=CH_2), 7·0–8·2 (12H, ArH).

1-(R)-[1-(S)-ethoxycarbonyl)ethoxycarbonyl]ethoxyphenyl 4′(11-propenoyloxyundecanoxy)biphenyl-4-carboxylate (**M2b**). Elemental analysis: calculated(found) for $C_{41}H_{50}O_{10}$: C 70·07(70·01), H 7·17(7·19). ^{1}H NMR ($CDCl_3$, TMS) δ (ppm): 1·25–1·9 (m, 27H, CH_3 and CH_2), 4·0 (t, 2H, $ArOCH_2$), 4·15–4·2 (m, 4H, CH_2=CH–$COOC\underline{H}_2$ and $COOC\underline{H}_2$–CH_3), 4·8 (q, 1H, ArOCH*), 5·15 (q, 1H, C$\underline{H}$*–$COOCH_2$), 5·8 and 6·4 (d, 2H, C$\underline{H}_2$=CH–COO), 6·1 (m, 1H, CH_2=C$\underline{H}$–COO), 6·95–8·20 (12H, ArH).

The copolysiloxanes (**CPS1** and **CPS2**) were prepared by classical hydrosilylation reactions between the vinylic mesogenic moieties (**M1a** and **M2a**) and a preformed poly(dimethylsiloxane-co-methylhydrosiloxane) having about 30% of reactive silane functions, in the presence of dicyclopentadienylplatinum(II) chloride as catalyst [36]. Similarly, the homopolysiloxanes (**HPS1** and **HPS2**) were prepared by hydrosilylation between the same mesogenic groups and a poly(methylhydrosiloxane). The starting poly(dimethylsiloxane-co-methylhydrosiloxane) [**PS123**] and poly(methylhydrosiloxane) [**PS120**] were purchased from Petrarch. The number-average molar mass (M_n) and the polydispersity index (I_p) of these starting polymers were determined by tonometry and permeation gel chromatography methods, respectively. The ratio of silane functions to siloxane units (expressed as a percentage x) in the copolysiloxanes was determined by ^{1}H NMR spectra. The investigation of the starting polysiloxanes gave the following characteristics: $M_n = 2280 \pm 200$ (M_n (manufacturer)=2270), I_p=1·4–1·5, x=25–35% (id. manufacturer) for **PS123** and $M_n = 2290 \pm 200$ (M_n (manufacturer)=2000–2100), I_p=1·2–1·3, for **PS120**.

The same procedure, which follows, was used to prepare the side group liquid crystalline copolysiloxanes (**CPS1**, **CPS2**) and homopolysiloxanes (**HPS1**, **HPS2**). A solution composed of a vinylic mesogenic moiety (**M1a** or **M2a**) [1·2 mmol] and a polysiloxane (1 mmol of Si–H function) in 15 ml of dry toluene was prepared. The mixture was heated at 80°C with argon bubbling for 20 min and then 100 µl of a solution of dicyclopentadienylplatinum(II) dichloride (1 mg ml^{-1} in dichloromethane) was injected. The solution was kept stirring and heated at that temperature under an argon atmosphere for two days. The resulting polymer was isolated from the unreacted vinylic mesogens by gel permeation chromatography (toluene as eluent, Ultrastyragel Bio-beads SX1, having a weight separation domain of 600–14 000), followed by a precipitation from a tetrahydrofuran solution into methanol. The polymer was dried *in vacuo* for 24 h at 60°C and 1 h at 100°C. Yield: 70–90%. For all polymers, the disappearance of the ^{1}H NMR peak corresponding to the Si–H group (δ=4·75 ppm) and integration of the various peaks confirmed that virtually all the Si–H bonds had been converted to Si–(mesogenic group). From the characteristic data obtained from the starting polysiloxanes, assuming first that all the Si–H groups have reacted and second that there has been no significant fractionation of the polymers during the synthetic procedure, the final polysiloxanes have the following characteristics: average degree of polymerization (D_{pn}) $= 30 \pm 4$ and 35 ± 5, for the copolysiloxanes and the homopolysiloxanes, respectively. In the copolysiloxanes, the percentage of siloxane groups functionalized by a mesogenic moiety (x) is 30 ± 5.

Copolysiloxane (**CPS1**). ^{1}H NMR ($CDCl_3$, TMS) δ (ppm): 0·10 (19·0H, $SiCH_3$), 0·5 (2H, $SiCH_2$), 0·9 (t, 3H, CH_3), 1·2–1·7 (m, 27H, CH_2 and CH*–C$\underline{H}_3$), 1·8 (m, 2H, C$\underline{H}_2$–CH_2O), 4·0 (t, 2H, CH_2OAr), 5·15 (q, 1H, C$\underline{H}$*), 6·9–8·3 (12H, ArH).

Copolysiloxane (**CPS2**). ^{1}H NMR ($CDCl_3$, TMS) δ (ppm): 0·10 (19·0H, $SiCH_3$), 0·5 (2H, $SiCH_2$), 1·2–1·45 (m, 17H, CH_2 and OCH_2–C$\underline{H}_3$), 1·5 (d, 3H, ArOCH*–C$\underline{H}_3$), 1·65 (d, 3H, C$\underline{H}_3$–CH*–$COOCH_2$), 1·8 (m, 2H, C$\underline{H}_2$–CH_2O), 4·0 (t, 2H, CH_2OAr), 4·2 (q, 2H, $OC\underline{H}_2$–CH_3), 4·8, (q, 1H, ArOCH*), 5·15 (q, 1H, C$\underline{H}$*–$COOCH_2$), 6·85–8·25 (12H, ArH).

Homopolysiloxane (**HPS1**). ^{1}H NMR ($CDCl_3$, TMS) δ (ppm): 0·10 (3·5H, $SiCH_3$), 0·55 (2H, $SiCH_2$), 0·85 (t, 3H, CH_3), 1·2–1·7 (m, 27H, CH_2 and CH*–C$\underline{H}_3$), 1·75

(m, 2H, C<u>H</u>$_2$–CH_2O), 3·95 (t, 2H, CH_2OAr), 5·15 (q, 1H, C<u>H</u>–CH_3), 6·9–8·3 (12H, ArH).

Homopolysiloxane (**HPS2**). ^{1}H NMR ($CDCl_3$, TMS) δ (ppm): 0·10 (3·5H, $SiCH_3$), 0·5 (2H, $SiCH_2$), 1·2–1·45 (m, 17H, CH_2 and OCH_2–C<u>H</u>$_3$), 1·5 (d, 3H, ArOCH*–C<u>H</u>$_3$), 1·65 (d, 3H, C<u>H</u>$_3$–CH*–$COOCH_2$), 1·8 (m, 2H, C<u>H</u>$_2$–CH_2O), 4·0 (t, 2H, CH_2OAr), 4·2 (q, 2H, OC<u>H</u>$_2$–CH_3), 4·8, (q, 1H, ArOCH*), 5·15 (q, 1H, C<u>H</u>*–$COOCH_2$), 6·85–8·25 (12H, ArH).

The side group liquid crystalline homopolyacrylates (**HPA1**, **HPA2**) were synthesized by a usual radical polymerization method from the mesogenic acrylate moieties (**M1b**, **M2b**) by using AIBN catalyst. The synthetic procedure is as follows: 1 mmol of acrylate monomer (**M1b**, **M2b**) was dissolved in 6 ml of dry toluene at room temperature; the solution was degassed by slight bubbling of argon for 20 min before 2 wt % of AIBN was introduced into the mixture. The polymerization was then carried out at 55°C for 24 h under an argon atmosphere. The reaction mixture was subjected to gel permeation chromatography (THF as eluent, Ultrastyragel Bio-beads SX1, having a weight separation domain of 600–14 000) and the polymers were fractionated by three successive precipitations from chloroform solution into ether. The polymers were dried in vacuo for 24 h at 60°C and 1 h at 120°C. Yield: 40–50%.

Homopolyacrylate (**HPA1**). ^{1}H NMR ($CDCl_3$, TMS) δ (ppm): 0·85 (t, 3H, CH_3), 1·15–1·55 (m, 24H, CH_2), 1·65 (d, 3H, CH*–C<u>H</u>$_3$), 1·75 (m, 4H, C<u>H</u>$_2$–CH_2O), 2·3 (1H, CH acrylic), 3·85–4·05 (4H, OCH_2), 5·15 (m, 1H, CH*), 6·85–8·25 (12H, ArH). The number-average molar mass (M_n = 57 000) and the weight-average molar mass (M_w = 120 000), as determined by analytical gel permeation chromatography (polystyrene standard), led to the calculated values of the average degree of polymerization (D_{pn}) of 85 $\pm$ 10 and a polydispersity index (I_p) of 2·10.

Homopolyacrylate (**HPA2**). ^{1}H NMR ($CDCl_3$, TMS) δ (ppm): 1·15–1·45 (m, 17H, CH_2 and $COOCH_2$–C<u>H</u>$_3$), 1·5 (d, 3H, ArOCH*–C<u>H</u>$_3$), 1·6 (d, 3H, C<u>H</u>$_3$–CH*–$COOCH_2$), 1·65–1·8 (4H, C<u>H</u>$_2$–CH_2O), 2·3 (1H, CH acrylic), 3·8–4·0 (m, 4H, CH_2OAr and $COOC$<u>H</u>$_2$–CH_2), 4·15 (q, 2H, $COOC$<u>H</u>$_2$–CH_3), 4·75 (q, 1H, ArOCH*), 5·1 (q, 1H, C<u>H</u>*–$COOCH_2$), 6·85–8·2 (12H, ArH). The number-average molar mass (M_n = 37 000) and the weight-average molar mass (M_w = 80 000), as determined by analytical gel permeation chromatography (polystyrene standard), led to the calculated values of the average degree of polymerization (D_{pn}) of 53 $\pm$ 6 and a polydispersity index (I_p) of 2·20.

2.2. *Characterization of the materials*

The chemical structure and the purity of the materials have been characterized using a number of techniques: thin layer chromatography (Whatman precoated silica gel 60-F_{254} plates), proton nuclear magnetic resonance spectroscopy (^{1}H NMR, Bruker MSL300) and elemental analysis. The starting polysiloxanes were characterized using tonometry and gel permeation chromatography on Ultrastyragel Waters columns: 10^4, 10^3 and 500 Å [solvent toluene, poly(methylhydro)siloxane standard]. The characteristics of the polyacrylates were determined by gel permeation chromatography on a Styragel microspher column: 10^3, 10^4 Å (solvent tetrahydrofuran, polystyrene standard). A Nikon polarizing microscope equipped with a Mettler hot stage was used to detect phase transition temperatures and to identify the mesophases from texture observations. Differential scanning calorimetry (Perkin-Elmer DSC7) was used to confirm the phase transition temperatures, as well as to record the transition temperatures to the more highly ordered phases and glass temperatures. The spontaneous polarization (P_s) was measured by the triangular wave method. A 20–100 V amplitude (frequency range 0·1–100 Hz) was applied across a 4-μm-thick sample, and the current was determined by measuring the voltage drop across a reference resistance with a storage oscilloscope.

3. Results

3.1. *Optical observations*

The phase sequences and associated transition temperatures of the materials were determined by thermal polarized light microscopy and differential scanning calorimetry. The results of these investigations for the LMM materials and for the polymers are given in tables 1 and 2, respectively.

3.1.1. *Low molecular weight compounds*

No specific surface treatment was needed for the texture observations of the monomers since large planar and pseudo-homeotropic coexisting regions could be obtained. The texture of the mesophases and accompanying transition temperatures for the low molecular mass materials were quite clear. As an example, the optical observations on **M2a**, which exhibits the phase sequence SmA–SmC*–SmC^*_γ–SmC^*_A–SmI^*_A, is reported here in detail.

On cooling an **M2a** sample from the SmA phase, a transition to the SmC* phase is observed: in the planar regions, a fan-shaped to a broken fan-shaped texture is established. The absence of dechiralization lines indicates the presence of a very short helical pitch. A typical texture for the SmC* phase is presented in figure 4. On further cooling in the SmC* phase, the pseudo-homeotropic regions present a first order selective reflection of the light which changes from red to blue continuously confirming, first, the presence of quite a small helical pitch and, secondly, revealing a slow

Table 1. Transition temperatures (°C) for the low molecular mass materials.

Substance	Phase																					
	Cr		SmI_A*		SmC_A*		SmC_γ*		SmC*		SmC_α*		SmA		N*		I					
MHBOBC	•	84·5	(•	65·3)	•	119·5	•	120·4	•	122·3	•	123·3	•	148·5			•					
M1a	•	59·7	(•	42·5)	•	118·9			•	120·7			•	134·3			•					
M1b	•	43·0			•	51·9	•	61·0	•	91·6			•	95·4			•					
M2	•	88·8			(•	47·0	•	50·6	•	70·0)			•	105·5			•					
M2a	•	61·8	(•	28·2	•	40·6	•	43·6)	•	70·6			•	95·4			•					
M2b	•	69·0					(•	31·0	•	63·6)			•	77·8	•	78·5[a]	•					

[a] With two blue phases included.

shortening of the helix pitch length with decreasing temperature. Then, cooling of the SmC* phase results in a transition to the SmC_γ^* phase. At the transition, a rapid unwinding of the helix occurs. The pseudo-homeotropic regions of the preparation exhibits a brief selective reflection of light, changing from blue to red, directly followed by grey domains in constant motion which finally coalesce (figure 5). In this schlieren texture of the SmC_γ^* phase a permanent motion of the disclination lines occurs. The SmC*–SmC_γ^* transition could also be detected from the appearance of coarse stripes in the broken focal-conics. As can be seen in figure 6, these stripes in the planar texture of the SmC_γ^* phase are similar to the stripes appearing in the textures of SmI* or SmF* phases. Further cooling produces a transition to the antiferroelectric SmC_A^* phase. In the planar alignment region, the coarse stripes vanish, while in the pseudo-homeotropic regions, the grey domains start moving again and disappear, accompanied by rapid selective reflection of the light again, revealing that the helix winds up rapidly. Typically, the SmC_A^* texture in **M2a** is composed of non-striated broken focal-conics (figure 7) and black pseudo-homeotropic regions. No significant modification in the texture was observed on cooling of the SmC_A^* phase to the more highly ordered phase. The changes in the selective reflection of the light observed on heating were the inverse of that seen on cooling, revealing that the winding and unwinding of the helix is a reversible process.

Circular dichroism investigations have also been performed on **M2a** and revealed that the helix is left-handed in the SmC* phase, while it is right-handed in the SmC_A^* phase. Such a change in the handedness of the helix between the SmC* and SmC_A^* phases has already been observed, as well as discontinuous jumps in the helical pitch length at the SmC*–SmC_γ^* and SmC_γ^*–SmC_A^* phase transitions (as described above from the optical observations) [7, 37, 38].

3.1.2. *Polymers*

As for the monomers, no specific surface treatment was needed for the texture observations of the polymers since large planar and large pseudo-homeotropic coexisting regions could be obtained.

On cooling from the isotropic phase the SmA phase appears in most of the polymers, showing a typical focal-conic fan shaped texture in the planar oriented regions. With the exception of the homopolyacrylate **HPA1**, further cooling of the SmA phase leads to a transition into the SmC* phase. At the SmA–SmC* transition temperature, the focal-conic fan-shaped texture of the SmA phase transforms into a broken focal-conic fan-shaped texture. Moreover, a colour change of the fans and the appearance of chirality lines were observed. In

Table 2. Transition temperatures (°C) for the polymers.

Substance	Phase													
	g		Cr[a]		Sm[b]		SmC_A*		SmC*		SmA		I	
CPS1	•	−7			•	9			•	136	•	155	•	
CPS2	•	−12			•	58[c]			•	91	•	122	•	
HPS1	•	33	•	52	(•	44)			•	189	•	213	•	
HPS2	•	12							•	172			•	
HPA1			•	85			•	159			•	191	•	
HPA2			•	80			•	127	•	129	•	161	•	

[a] Crystalline phase or high ordered smectic phase.
[b] Undetermined ordered smectic phase.
[c] Probably SmI* or SmF* phase.

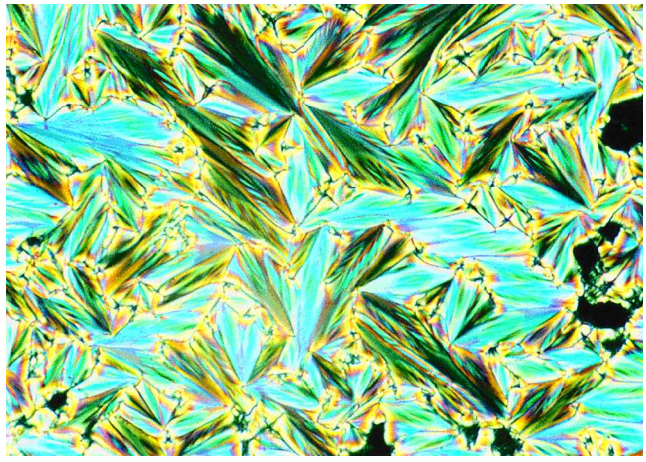

Figure 4. Photomicrograph of the texture of **M2a** in the SmC* phase, at 60°C (magnitude ×40).

the pseudo-homeotropic regions a non-specific schlieren texture appears at the SmA–SmC* transition. For the polymer **HPS2**, which shows a direct transition from the isotropic into the SmC* phase, a similar texture of the SmC* phase was found. Both homopolyacrylates exhibit a further smectic modification which, on the basis of miscibility studies, was classified as the SmC_A^* phase. The texture of this phase is similar to the texture of the SmC* phase. In the planar oriented regions a broken focal-conic fan-shaped texture and in the pseudo-homeotropic regions a non-specific schlieren texture were obtained. At the SmC* to SmC_A^* phase transition of the polymer **HPA2**, a colour change of the broken focal-conic fans and an increase of the number of chevron defects were observed, as is typical for a SmC* to SmC_A^* transition. However, the texture was too

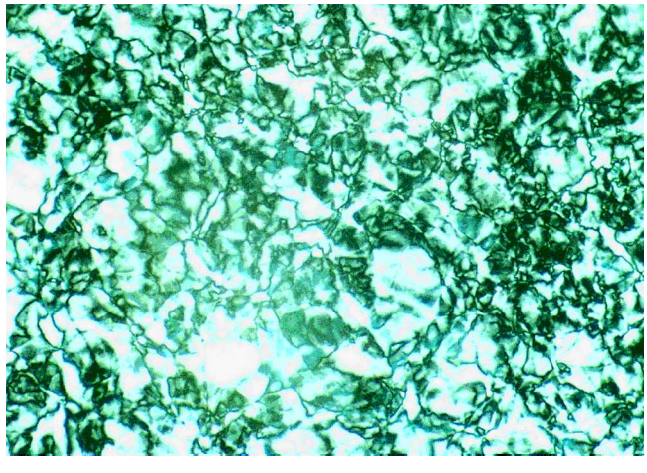

Figure 5. Photomicrograph of a pseudo-homeotropic region of the LMM material **M2a** at the SmC*–SmCγ* phase transition, at 43·5°C (magnitude ×40).

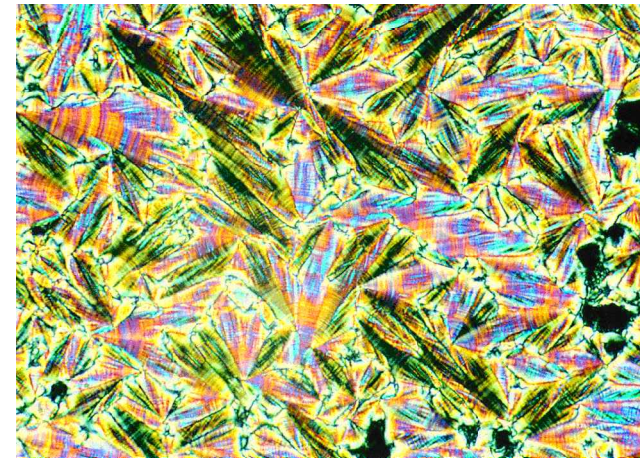

Figure 6. Photomicrograph of the texture of the LMM material **M2a** in the SmCγ* phase, at 42°C (magnitude ×40).

unspecific for a classification of the SmC_A^* phase just on the basis of texture observations

3.2. *Miscibility studies*

Miscibility studies were systematically performed for each LMM material and polymer reported here. These investigations were carried out for the monomers by making mixtures with the (*R*)- or/and the (*S*)-enantiomer of **MHPOBC**, while for the polymers, the mixtures were made with their low molecular mass analogues, **M1a** or **M2a**. The phase diagrams thus obtained helped us to determine the stability of the antiferroelectric and ferrielectric smectic phases in the pure materials.

3.2.1. *Low molecular mass materials*

Three phase diagrams resulting from the miscibility studies for the LMM materials are given below: **M2a** with (*R*)-**MHPOBC** (figure 8), **M2a** with (*S*)-**MHPOBC**

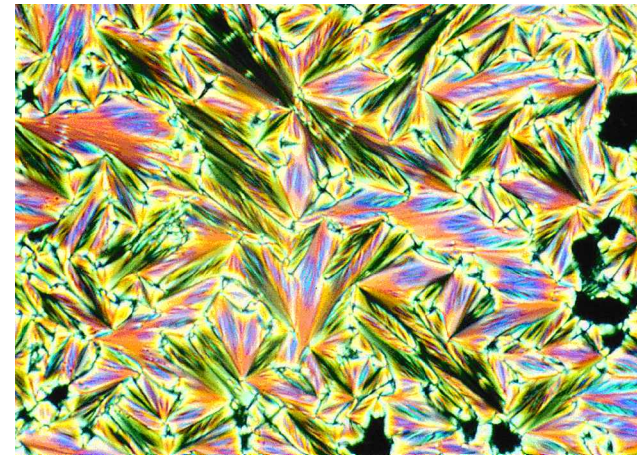

Figure 7. Photomicrograph of the texture of the LMM material **M2a** in the SmC_A^* phase, at 34°C (magnitude ×40).

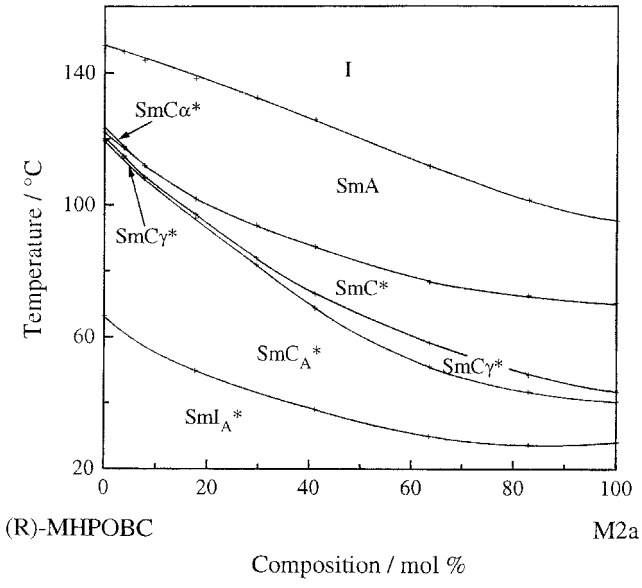

Figure 8. Miscibility phase diagram between the (*R*)-**MHPOBC** and the LMM mesogen **M2a**.

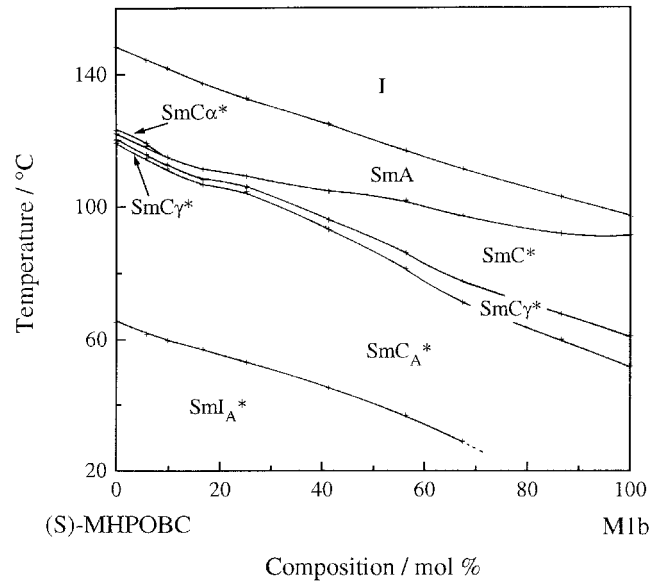

Figure 10. Miscibility phase diagram between (*S*)-**MHPOBC** and the LMM mesogen **M1b**.

(figure 9) and the acrylate **M1b** with (*S*)-**MHPOBC** (figure 10).

In the phase diagram presented in figure 8, we observe that the SmC^*_γ and SmC^*_A phases of **M2a** and (*R*)-**MHPOBC** are miscible, and are present over the entire concentration range of both components. In contrast, the SmC^*_α phase of (*R*)-**MHPOBC** disappears rapidly when adding only a few mol% of **M2a** (the strong destabilization of the SmC^*_α phase was generally observed for each LMM material synthesized in this work in mixtures with **MHPOBC**). On further increasing the concentration of **M2a** in (*R*)-**MHPOBC**, all the transition temperatures change continuously towards those of pure **M2a**: however, the SmC* phase temperature range expands and disfavours that of the SmC^*_A phase, while the temperature range of SmC^*_γ enlarges in the mixtures and then decreases to reach a 3°C temperature range in **M2a**. The SmI^*_A phase present in (*R*)-**MHPOBC** was also miscible with the most highly ordered phase of **M2a**, and since the SmC^*_A–SmI^*_A phase transition line could be followed monotonously in the mixtures from (*R*)-**MHPOBC** to **M2a**, we assume that the most highly ordered phase in **M2a** is SmI^*_A (the same assumption was made for the compound **M1a**).

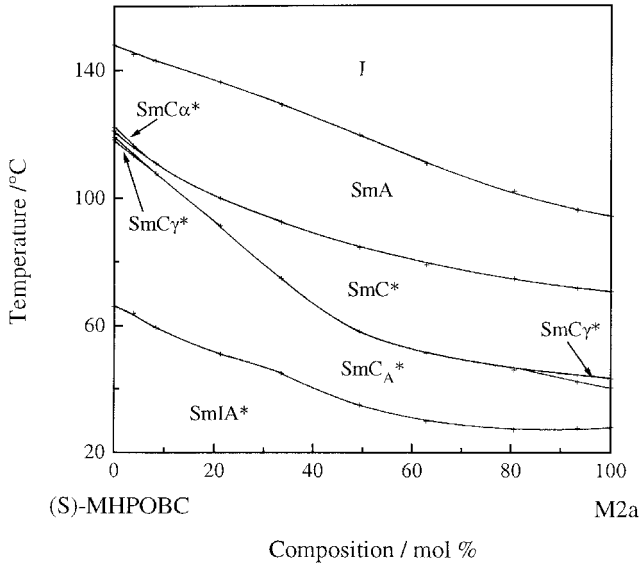

Figure 9. Miscibility phase diagram between the (*S*)-**MHPOBC** and the LMM mesogen **M2a**.

The phase diagram between the same LMM material **M2a** with (*S*)-**MHPOBC** (figure 9) is similar to that previously presented with the (*R*)-enantiomer of **MHPOBC**, except for the SmC^*_γ phase which was found only at high concentrations of one other of the pure components. Such destabilization of the SmC^*_γ has already been observed in mixtures between (*S*)- and (*R*)-**MHPOBC**, without explanation of its origin [27]. Here, the disappearance of the SmC^*_γ in the mixtures between (*S*)-**MHPOBC** and **M2a** seems to be due to an increase of the helical pitch (since the SmC^*_γ phase of each material is of opposite handedness) rather than to a change in their chirality (the two materials have the same sign of spontaneous polarization).

The phase diagram between (*S*)-**MHPOBC** and **M1b** (figure 10) shows a continuous depression of the transition temperature lines. The SmC^*_γ and SmC^*_A phases of both materials are miscible over all concentrations of the mixtures. In adding **M1b** into (*S*)-**MHPOBC**, the

SmC^*_α phase disappears rapidly; then we observe that the temperature ranges of the SmC* and SmC^*_γ phases increase and that of the SmA phase decreases. In pure **M1b**, a temperature range of nearly 10°C is obtained for the SmC^*_γ phase. Finally, because of crystallization of the mixtures, the SmC^*_A–SmI^*_A phase transition line could not be followed above 70 mol % of **M1b** in (*S*)-**MHPOBC**.

3.2.2. *Polymers*

Binary phase diagrams have been constructed for each polymer with its respective LMM analogue **M1a** or **M2a**. The phase diagrams corresponding to the copolysiloxanes **CPS1** and **CPS2**, the homopolysiloxanes **HPS1** and **HPS2**, and the homopolyacrylates **HPA1** and **HPA2** are reported in figures 11–16, respectively.

As a first observation, the miscibility phase diagrams corresponding to both copolysiloxanes (figures 11 and 12) show that the SmC^*_A phase is rapidly suppressed in mixtures when about 20–30 wt % of copolymer is added to its related LMM material. The same observation is made for the SmC^*_γ phase in the binary mixture **M2a**–**CPS2**. On the other hand, both phase diagrams reveal, below the SmA phase, a stabilization of the SmC* phase and an unclassified, more ordered smectic phase (probably SmI* or SmF*). It is interesting to note that the higher ordered phase of the copolysiloxane **CPS2**, which is found to be a ferroelectric phase (see spontaneous polarization measurements), appears between the SmC* and SmI^*_A phase. So far and to our knowledge, only one binary system has been reported exhibiting a

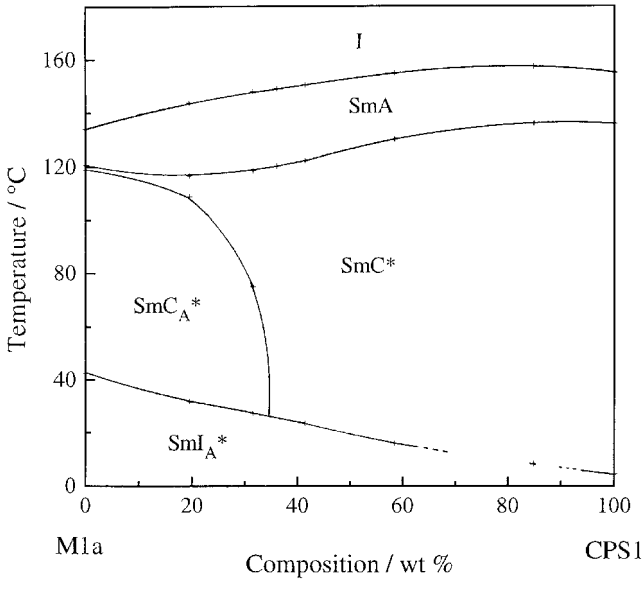

Figure 11. Miscibility phase diagram between the copolysiloxane **CPS1** and its low molecular mass analogue **M1a**.

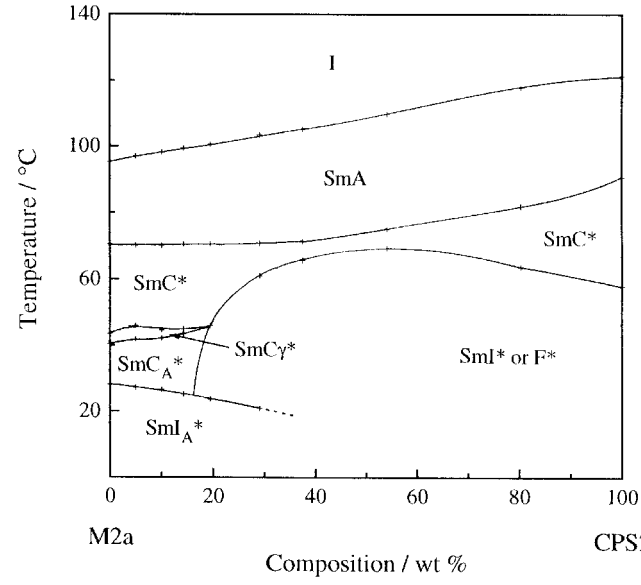

Figure 12. Miscibility phase diagram between the copolysiloxane **CPS2** and its low molecular mass analogue **M2a**.

phase transition between a higher ordered ferroelectric and a higher ordered antiferroelectric phase. In that binary system, the SmI* phase has been found to be the *low* temperature phase of the SmI^*_A phase [39].

As for the copolysiloxanes, the phase diagrams corresponding to the homopolysiloxanes (figures 13 and 14) show a strong destabilization of the SmC^*_A and SmC^*_γ phases on increasing the concentration of the polymers in the related LMM materials. Only a 10–20 wt % concentration of polymer is enough to suppress the

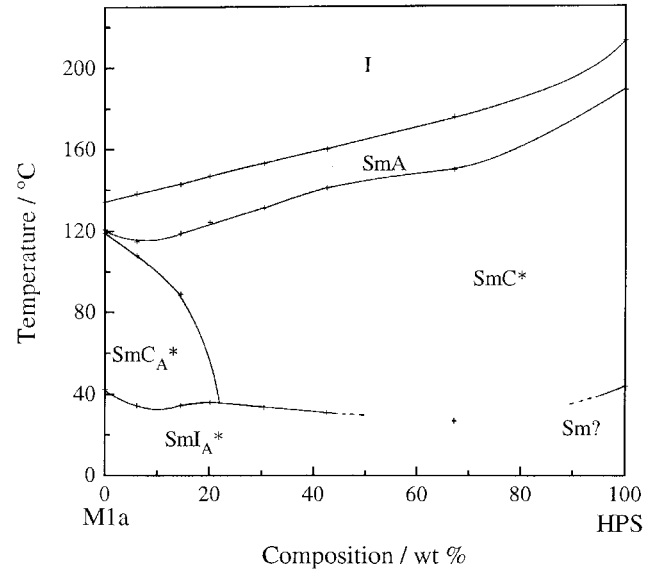

Figure 13. Miscibility phase diagram between the homopolysiloxane **HPS1** and its low molecular mass analogue **M1a**.

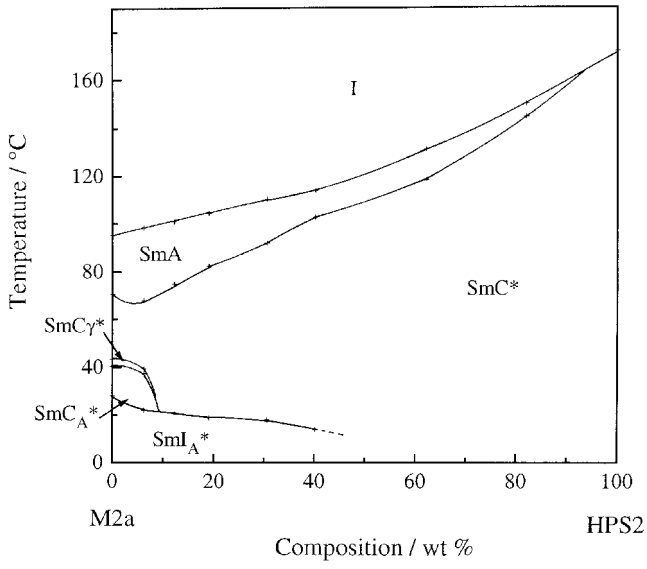

Figure 14. Miscibility phase diagram between the homopolysiloxane **HPS2** and its low molecular mass analogue **M2a**.

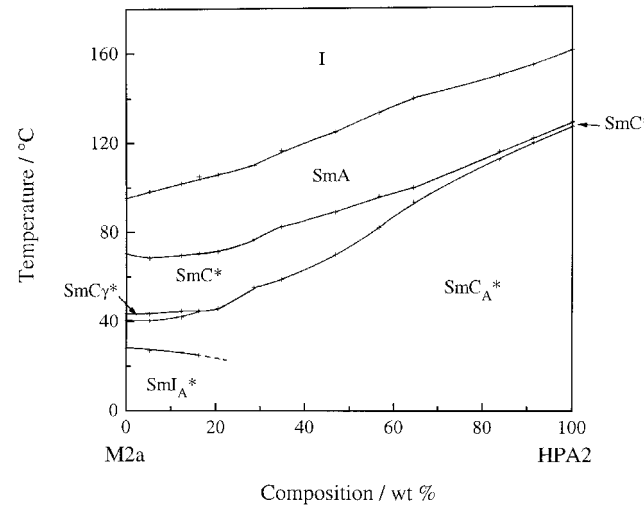

Figure 16. Miscibility phase diagram between the homopolyacrylate **HPA2** and the LMM material **M2a**.

antiferro- and ferri-electric phases. This destabilization effect is more pronounced in the case of the homopolysiloxane **HPS2** than for **HPS1**. In going to higher concentrations of polymer, the SmC* phase is found to be more and more stabilized, so that in the pure **HPS**2, e.g. it is the only mesophase present.

Contrary to the phase diagrams previously cited, the binary mixtures of the homopolyacrylates **HPA1** and **HPA2** with the related LMM materials (figures 15 and 16, respectively) show that the SmC_A^* phase is present for all concentrations. Thus, the SmC_A^* phase remains present in both pure homopolyacrylates, and over a large temperature range. This antiferroelectric phase is limited at the lower temperature end by the existence of a high order (or crystalline) phase. As regards the SmC_γ^* phase, the same observation is made for the copolysiloxane **CPS2**, homopolysiloxane **HPS2** and homopolyacrylate **HPA2**: the SmC_γ^* phase is still strongly destabilized in mixtures, and is suppressed for a polymer concentration as small as 20 wt % of **CPS2** and **HPA2** in the LMM materials. On the other hand, the temperature range of the usual ferroelectric SmC* phase is found to be more and more reduced when going from the pure LMM materials to the polymers: the SmC* phase is finally totally suppressed in **HPA1**, while it remains present over a very narrow temperature range in the polymer **HPA2**. For the homopolyacrylates, the SmC_A^*–SmI_A^* transition line could not be followed in the mixtures for polymer concentrations above 40 wt % with **M1a** and above 15 wt % with **M2a**.

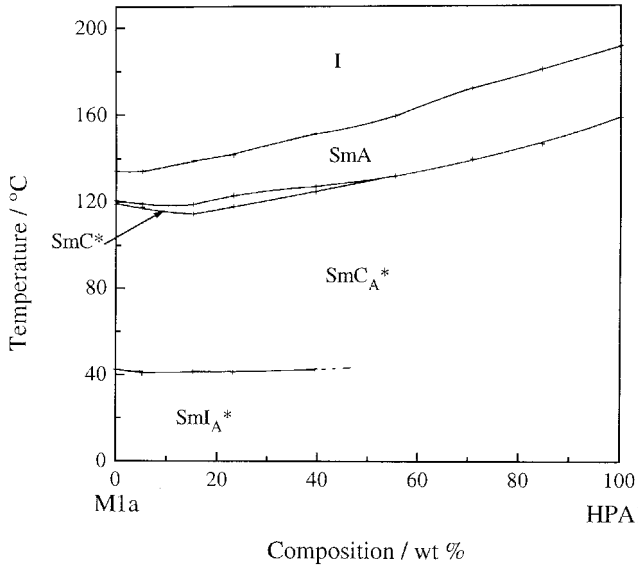

Figure 15. Miscibility phase diagram between the homopolyacrylate **HPA1** and the LMW material **M1a**.

3.3. *Calorimetry studies*

Differential scanning calorimetry (DSC) was systematically used to confirm the phase transition temperatures and to quantify their associated enthalpies. As a first result, and as previously observed in **MHPOBC** and in a series of **MHPOBC** derivatives, the SmC*–SmC_γ^*, SmC_γ^*–SmC_A^* and direct SmC*–SmC_A^* phase transitions are accompanied by a very weak (or even undetectable) enthalpy variation [34, 38]. In our materials, these enthalpies are generally weaker than 0·1 KJ mol^{-1}. However, an enthalpy as large as 4·0 KJ mol^{-1} was measured for the SmC*–SmC_A^* transition in the homopolyacrylate **HPA2**. Three thermograms are given here as examples: the thermograms correspond to compounds

M1a (figure 17) and **M2a** (figure 18), recorded on cooling at 2°C min^{-1} and to the homopolyacrylate **HPA2**, recorded on cooling at 5°C min^{-1} (figure 19).

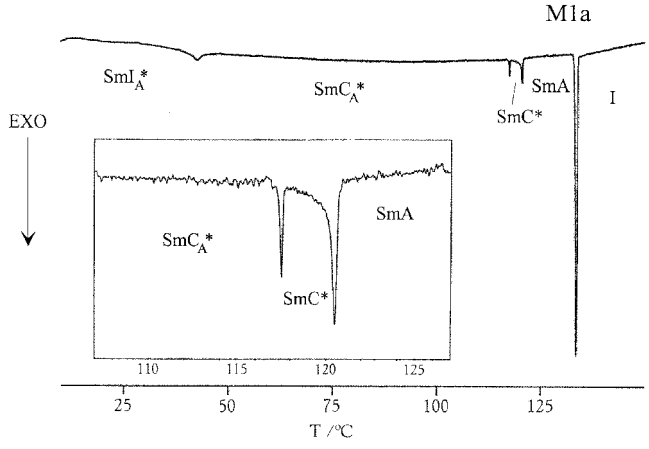

Figure 17. DSC thermogram of **M1a**, recorded on cooling at 2°C min^{-1}.

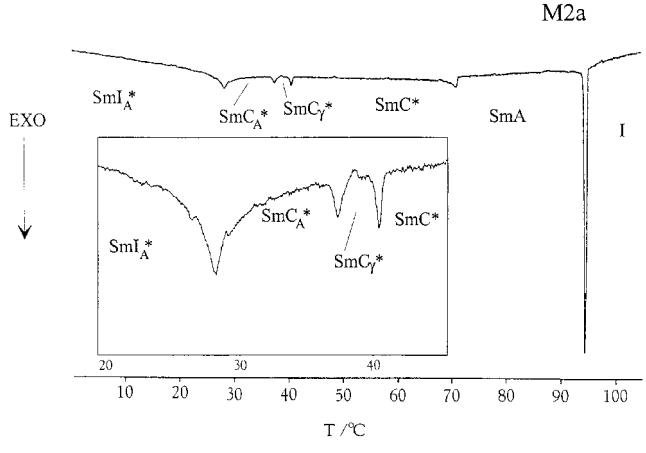

Figure 18. DSC thermogram of **M2a**, recorded on cooling at 2°C min^{-1}.

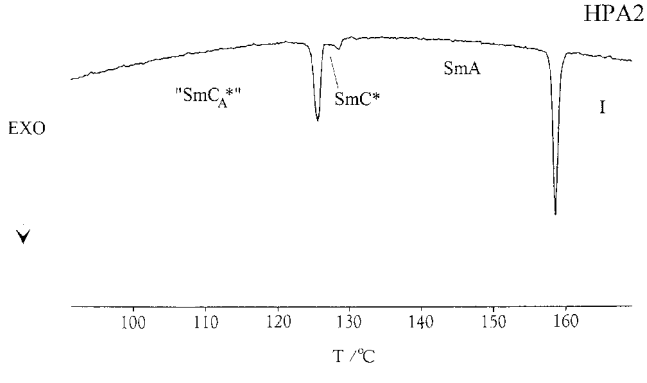

Figure 19. DSC thermogram of the homopolyacrylate **HPA2**, recorded on cooling at 5°C min^{-1}.

3.4. *Spontaneous polarization measurements*

Spontaneous polarization (P_s) measurements have been carried out for the materials. However, no attempt was made to investigate the LMM acrylates, the homopolysiloxanes and the homopolyacrylates; with the acrylates this was because of the risk of thermal polymerization during the cell filling process, and with the homopolymers because of the high melt viscosity and clearing temperatures for filling the cells by capillarity. Spontaneous polarization has been measured by using the triangular wave method [40], with 4-μm-thick cells. The applied electric field was chosen to be strong enough to produce a fully poled ferroelectric state, even in the antiferroelectric phase. The temperature dependence of P_s for the LMM compounds **M1a** and **M2a** are given in figures 20 and 21, respectively. Because of the high electric field used, no discontinuity in the evolution of P_s was found when passing through the SmC^*_γ or

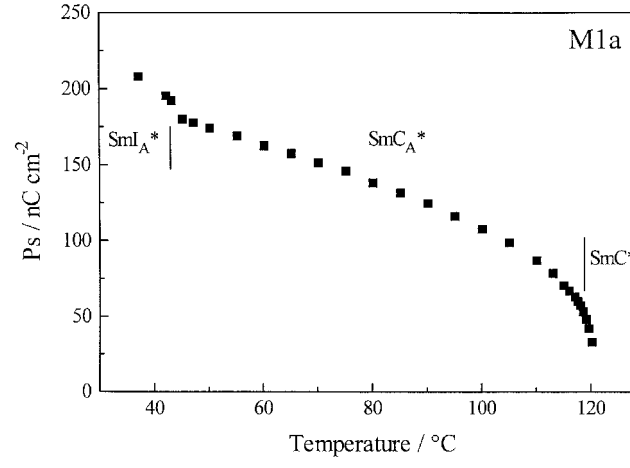

Figure 20. Temperature dependence of the spontaneous polarization for the LMM mesogen **M1a**.

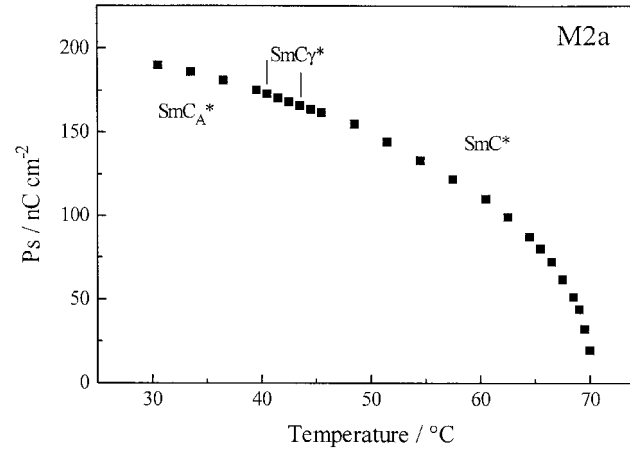

Figure 21. Temperature dependence of the spontaneous polarization for the LMM mesogen **M2a**.

SmC_A^* phases. The values observed for P_s are high and saturate to about 200 nC cm^{-2}, for both materials.

The variation of P_s for the copolysiloxanes **CPS1** and **CPS2** are given in figures 22 and 23, respectively. The evolution of P_s for **CPS1** is quite similar in values to that observed for its LMM analogue **M1a** (figure 20), except that a smoother increase of P_s occurs for **CPS1** below the SmA–SmC* transition which is due to an inhomogeneity of the transition temperatures. A drastic change is observed for the copolysiloxane **CPS2** (figure 23). However, when it is compared to its related LMM compound **M2a** (figure 21), the temperature dependence of P_s for **CPS2** reveals much lower values in the SmC* phase than for compound **M2a** in the same mesophase. Surprisingly, the high order mesophase of **CPS2** reveals quite high values of P_s, reaching up to 450 nC cm^{-2} at low temperatures. This higher ordered mesophase was found to be ferroelectric (most probably a SmI* or F* phase), as observed by electro-optical investigations from the presence of a single current peak and bistable switching.

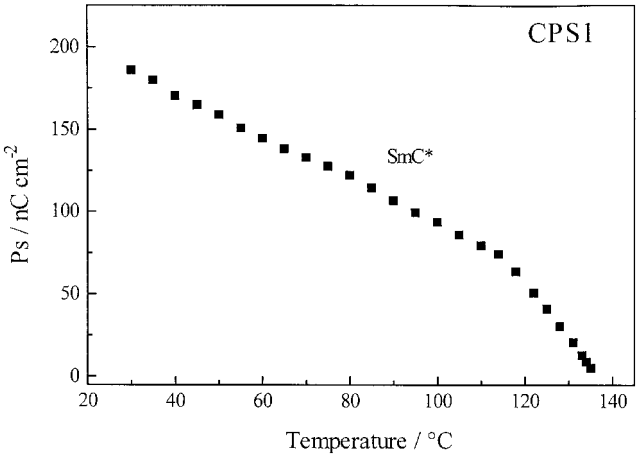

Figure 22. Temperature dependence of the spontaneous polarization for the copolysiloxane **CPS1**.

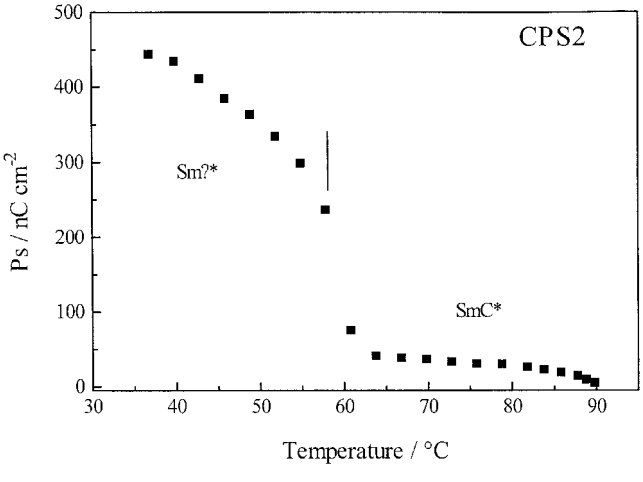

Figure 23. Temperature dependence of the spontaneous polarization for the copolysiloxane **CPS2**. (Sm?*: most probably SmI* or F* phase.)

3.5. *Electro-optical investigations*

The electro-optical investigations of the SmC_A^* phase were carried out only for the vinylic systems **M1a** and **M2a**. No electro-optical study was made on the homopolyacrylates because their high melt viscosity and clearing temperature made filling the measurement cells impracticable.

Evidence of the tristable switching process in the antiferroelectric smectic phase (SmC_A^*) of **M1a** is given in figure 24. Applying a triangular wave voltage as shown in figure 24 (*b*) (frequency = 12 Hz, voltage = 29 V) across a 4-μm-thick sample at 80°C produced the transmittance signal (between crossed polarizers) given in figure 24 (*a*) [12]. This optical response clearly shows a tristable switching process: a third state (antiferroelectric) is observed at lower electric field between the two ferroelectric states. The current peaks associated with the ferroelectric–antiferroelectric switching are presented in figure 24 (*c*). Such investigations have been attempted for the SmC_A^* phase of pure **M2a** without any success because of strong anchoring of the helix. Between the two ferroelectric states, we observed optically the winding and unwinding processes of the helix which could not be eliminated even by reducing the cell thickness to 2 μm. However, the ferroelectric–antiferroelectric switching could be observed in the SmC_A^* phase of a

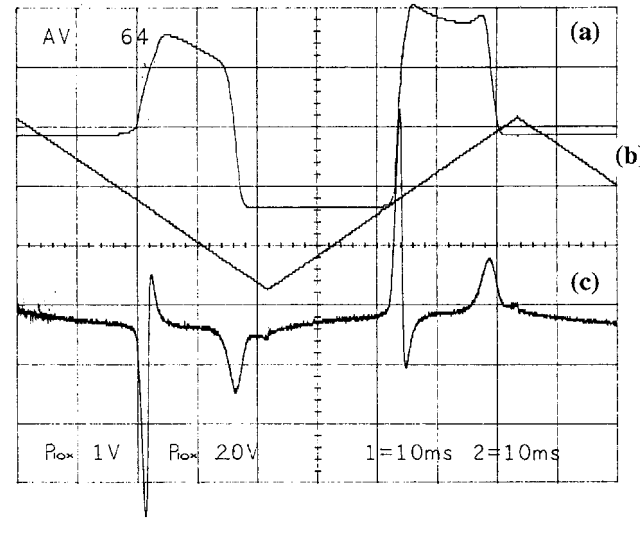

Figure 24. Light transmittance (*a*) and switching current responses (*c*) to a triangular wave form (*b*) observed at 80°C in the SmC_A^* phase of **M1a**.

50 mol % mixture of **M2a** with (*R*)-**MHPOBC** (see phase diagram presented in figure 8).

4. Discussion

First, let us discuss the stability of the antiferro- and ferri-electric mesophases in the LMM compounds. Both SmC_A^* and SmC_γ^* phases are present in the lactate-based liquid crystalline materials. The appearance of these mesophases seems to be due to the combination of the two lactate groups constituting the chiral moiety. Previous work has shown that when the second chiral lactate group is replaced by *n*-hexyl [figure 25 (*a*) or a chiral 1-methylheptyl (figure 25 (*b*)] chain, the molecules exhibit neither the SmC_A^* nor the SmC_γ^* phase [41]. It has to be noted however that the SmC_A^* phase could possibly be present in the latter case, but would have to be strongly metastable in relation to the crystalline phase. On the other hand, the carboxy (COO) linking group between the aromatic core and the chiral part apparently do not seem to increase the ability to produce the formation of the SmC_A^* phase. As a matter of fact, the compound presented in figure 25 (*c*) does not exhibit the antiferroelectric phase [41]. However, lengthening of the aliphatic chain located at the end of the chiral part would probably favour the formation of SmC_A^*, as has already been observed in other antiferroelectric liquid crystalline systems [16, 38, 42]. The results presented above show that the antiferroelectric phase seems to be stabilized by a strongly polar chiral group, which is constituted by the presence of three successive dipole moments carried by the oxygen linking atom and the two carboxylate groups. This observation, associated with the large values of the saturated spontaneous polarization in the SmC* phase obtained for the LMM materials (as well as for the **MHPOBC** derivatives), is in agreement with the postulate of the pairing of molecules in the formation of the antiferroelectric mesophases [14, 15]. Thus, the antiferroelectric mesophase in our materials might possibly be stabilized by a pairing association of the strongly polarized chiral parts of the molecules in adjacent smectic layers.

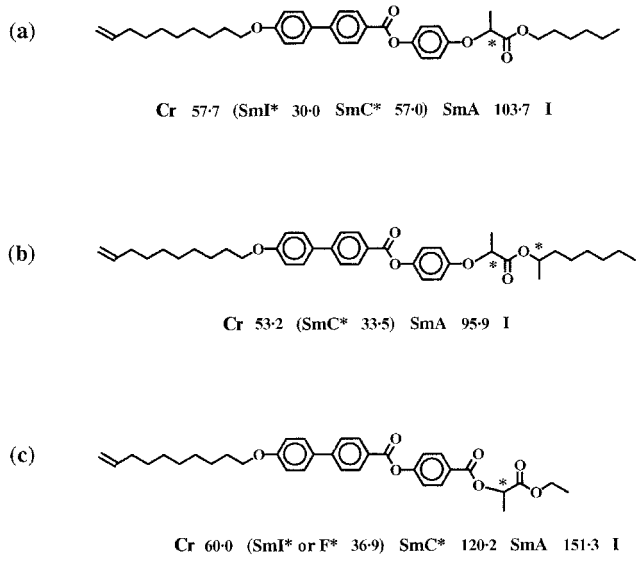

Figure 25. Lactate-based ferroelectric liquid crystals.

The difference in the mesomorphic properties of the materials can be observed from the values of the transition temperatures reported in table 1. The major difference between the **MHPOBC** related and lactate-based compounds is that the latter exhibit (with the exception of the melting points), much lower transition temperatures. For instance, the clearing point is decreased by about 40°C in **M2**, compared with **M1**. Another tendency to mention is that the SmC_A^* phase seems to be more stabilized in the **MHPOBC** derivatives than in the lactate-based compounds. A possible explanation of this destabilization effect might be related to a weaker correlation of the chiral part with the rigid core when the carboxy linking group is replaced by an oxygen. Some authors underline the importance of the presence of the carboxy linking group in the formation of antiferroelectric mesophases through restriction of free rotation of the dipole moment located in the vicinity of the chiral centre [42, 43].

Let us examine the effect of molecular change to a paraffin chain. It is well known that any structural change to a pure hydrogenous alkyl chain in a liquid crystal will cause a destabilization of the mesomorphic properties. It is generally assumed that the more important the molecular change, the larger the thermal destabilization.

As a first observation, the addition of a vinyl group to the saturated aliphatic tail in liquid crystal materials produces a shift of the melting and clearing points towards lower temperatures. A similar effect has already been obtained by Kelly in particular, for mesogens having unsaturated aliphatic chains [44]. In relation to this destabilization effect, the disappearance of the SmC_α^* and SmC_γ^* phases in the vinylic analogue of **MHPOBC** must be mentioned, confirming that these novel mesophases are very sensitive to slight modifications in molecular structure [22, 26, 38, 42].

The replacement of the saturated alkyl chain by an acryloxy-terminated alkyl chain corresponds to the introduction of a bulky and polar end group. The incorporation of such a group in our molecules causes a strong decrease in the thermal stability of the mesophases. Surprisingly however, this molecular change stabilizes the SmC_γ^* phase: the temperature range of the SmC_γ^* phase is expanded in both acrylate compounds, to reach a value of about 10°C in compound **M1b**, in particular. The thermal destabilization effect caused by

the introduction of a terminal acryloxy group has already been observed in antiferroelectric mesogens [22]. In these materials however, the authors have observed that the SmC_A^* phase is less destabilized than the other mesophases, which is not the case for our materials.

As regards the polymeric materials, the stability of the mesophases as a function of the nature of the polymer backbone can be observed from the mesomorphic sequences and transition temperatures of the polymers reported in table 2. First, the mesomorphic properties are stabilized upon polymerization. This behaviour, well known in liquid crystalline polymers, is reflected by the increase of the value of the clearing points (and also the mesomorphic temperature ranges) in polymers as compared with their corresponding low molecular mass mesogens [45]. Because of the 'dilution' of the mesogenic pendants on the polysiloxane backbone, the copolysiloxanes exhibit clearing points intermediate between those observed for the homopolysiloxanes and for the starting mesogens [46, 47].

The more striking result concerns the stability of the antiferroelectric mesophase in the polymers. By means of miscibility studies, the SmC_A^* phase is found to be strongly stabilized over the SmC* phase in the homopolyacrylates, while opposite results are obtained for the polysiloxanes, where no antiferroelectric phase is observed. From the miscibility phase diagrams, it is also clear that the antiferroelectric mesophases appear to be more destabilized in the homopolysiloxanes than in the copolysiloxanes. The difference in stability of the SmC_A^* phase in the polymers is quite surprising since it seems to rely only on the nature of the polymer backbone, in spite of the decoupling action of the spacer.

The stabilization of the SmC_A^* phase upon polymerization has recently been observed by Nishiyama and Goodby [22]. The polymers they investigated were based only on a polyacrylate backbone; their polymers were prepared by radical polymerization, by using a similar procedure to ours. Their materials were characterized by a degree of polymerization (D_{pn}) lower than 20, and thus should be regarded more as oligomers than polymers. However, these authors have observed that the antiferroelectric mesophase was strongly stabilized upon polymerization, in such a way that the polyacrylates exhibit, below the SmA phase, only the SmC_A^* phase over a large temperature range. On the contrary, a series of side group liquid crystalline oligosiloxanes prepared from antiferroelectric mesogens has been reported in the literature, in which the oligomers exhibit only the classical ferroelectric SmC* phase [48].

Nishiyama and Goodby gave two possible explanations for the stabilization of the antiferroelectric phase in the polyacrylates [22]. First, as for the low molecular weight compounds, the stabilization of the antiferroelectric order in the polymers could be due to the molecular dipole–dipole interactions. Because the polymer liquid crystals can be seen as a 'cluster' of monomers, the dipole–dipole interactions between the clusters can be considered to be stronger in the polymers than in the starting LMM materials. If this explanation is valid for the polymers, it is still unclear why the stabilization of the antiferroelectric phase varies so greatly between two homopolymers (homopolyacrylates and homopolysiloxanes) which differ only in the nature of the polymer backbone.

The second proposed explanation lay in the conformational shape of the backbone of the polymer, determining the orientation of the appended mesogenic moieties relative to the backbone itself. It has to be noted that the conformational aspect governing the antiferroelectric order has already been observed in the case of main chain polymers and in some dimeric compounds [31, 32]. In side group liquid crystalline polymers, one can reasonably assume that the stabilization of the antiferroelectric ordering can be produced only if the polymer backbone has a tendency to a specific stereoregularity. However, several publications have revealed that ramified polymethylsiloxanes [49, 50] as well as radically polymerized polyacrylates [51] give atactic polymers. In the latter case, atacticity was observed even for radical polymerization of bulky monomers [51–54].

Finally, as has been commonly observed in antiferroelectric polymers, the SmC_γ^* appears to be strongly destabilized upon polymerization. The reason why the ferrielectric phase is unstable in polymeric materials remains puzzling.

5. Conclusion

We have prepared and examined the mesomorphic properties of LMM materials and side group polymers. All the LMM materials exhibit antiferroelectric SmC_A^* and/or the ferrielectric SmC_γ^* mesophases. For the side-chain polymers, only the macromolecules having a homopolyacrylate backbone exhibit most probably the SmC_A^* phase, while the polymers having a copolysiloxane or homopolysiloxane backbone exhibit only the classical ferroelectric SmC* phase. On the other hand, no SmC_γ^* phase is found in any polymer. The effects of the molecular structure on the stabilization of the antiferroelectric (and ferrielectric) mesophases are still far from understood. For the polymeric materials in particular, it is still unclear whether the appearance of the antiferroelectric phases is caused by dipole–dipole interactions, conformational order of the polymer backbone, or other reasons. It would be of great interest to investigate fully the stereoregularity of antiferroelectric and ferroelectric polymers, in order to examine the influence (or not) of

the steric aspect on the formation of antiferroelectric phases. On the other hand, it would be interesting to vary the length of the spacer in the antiferroelectric side chain polymers, to observe whether the conformational aspect of the spacer plays a specific role in the stability of the antiferroelectric phase. Finally, in order to permit a full (optical and electro-optical) characterization of the antiferroelectric macromolecules, it will be necessary to prepare oligomeric materials, instead of high molecular weight polymers.

We are grateful to J. Naciri, J. Hollidt and P. Keller for stimulating and fruitful discussions, as well as to M. Mauzac for the characterization of the starting polysiloxanes. We would like to thank the Deutsche Forschungsgemeinschaft (Sonderforschungsbereich 335, 'Anisotrope Fluide') for financial support.

References

[1] Fukuda, A., Takanishi, Y., Isozaki, T., Ishikawa, K., and Takezoe, H., 1994, *J. mater. Chem.*, **4,** 997.
[2] Chandani, A. D. L., Ouchi, Y., Takezoe, H., Fukuda, A., Terashima, K., Furukawa, K., and Kishi, A., 1989, *Jpn. J. appl. Phys.*, **28,** L1261.
[3] Levelut, A. M., Germain, C., Keller, P., Liébert, L., and Billard, J., 1983, *J. Phys.*, **44,** 623.
[4] Galerne, Y., and Liébert, L., 1991, *Phys. Rev. Lett.*, **66,** 2891.
[5] Heppke, G., Kleineberg, P., Lötszch, D., Méry, S., and Shashidhar, R., 1993, *Mol. Cryst. liq. Cryst.*, **231,** 257.
[6] Takanishi, Y., Takezoe, H., Johno, M., Yui, T., and Fukuda, A., 1993, *Jpn. J. appl. Phys.*, **32,** 4605.
[7] Chandani, A. D. L., Gorecka, E., Ouchi, Y., Takezoe, H., and Fukuda, A., 1989, *Jpn. J. appl. Phys.*, **28,** L1265.
[8] Galerne, Y., and Liébert, L., 1990, *Phys. Rev. Lett.*, **64,** 906.
[9] Gorecka, E., Chandani, A. D. L., Ouchi, Y., Takezoe, H., and Fukuda, A., 1990, *Jpn. J. appl. Phys.*, **29,** 131.
[10] Zeks, B., Blinc, R., and Cepic, M., 1991, *Ferroelectrics*, **122,** 221.
[11] Zeks, B., and Cepic, M., 1993, *Liq. Cryst.*, **14,** 445.
[12] Chandani, A. D. L., Hagiwara, T., Suzuki, Y. I., Ouchi, Y., Takezoe, H., and Fukuda, A., 1988, *Jpn. J. appl. Phys.*, **27,** L729.
[13] Lee, J., Chandani, A. D. L., Itoh, K., Ouchi, Y., Takezoe, H., and Fukuda, A., 1990, *Jpn. J. appl. Phys.*, **29,** 1122.
[14] Takanishi, Y., Hiraoka, K., Agrawal, V. K., Takezoe, H., Fukuda, A., and Matsushita, M., 1991, *Jpn. J. appl. Phys.*, **30,** 2023.
[15] Isozaki, T., Fujikawa, T., Takezoe, H., Fukuda, A., Hagiwara, T., Suzuki, Y., and Kawamura, I., 1993, *Phys. Rev. B.*, **48,** 13439.
[16] Ikeda, A., Takanishi, Y., Takezoe, H., and Fukuda, A., 1993, *Jpn. J. appl. Phys.*, **32,** L97.
[17] Decobert, G., Dubois, J. C., Esselin, S., and Noël, C., 1986, *Liq. Cryst.*, **1,** 307.
[18] Davidson, P., Kühnpast, K., Springer, J., and Scherowsky, G., 1993, *Liq. Cryst.*, **14,** 901.
[19] Bömelburg, J., Heppke, G., and Hollidt, J., 1991, *Makromol. Chem., rapid Commun.*, **12,** 483.
[20] Gießelmann, F., Zugenmaier, P., Scherowsky, G., Kühnpast, K., and Springer, J., 1992, *Makromol. Chem., rapid Commun.*, **13,** 489.
[21] Skarp, K., Andersson, S. T., Lagerwall, S. T., Kapitsa, H., Poths, H., and Zentel, R., 1991, *Ferroelectrics*, **122,** 127.
[22] Nishiyama, I., and Goodby, J. W., 1993, *J. mater. Chem.*, **3,** 169.
[23] Watanabe, J., Hayashi, M., Morita, A., and Niiori, T., 1994, *Mol. Cryst. Liq. Cryst.*, **254,** 221.
[24] Mensinger, H., Biswas, A., and Poths, H., 1992, *Macromolecules*, **25,** 3156.
[25] Takezoe, H., Fukuda, A., Ikeda, A., Takanishi, Y., Umemoto, T., Watanabe, J., Iwane, H., Hara, M., and Itoh, K., 1991, *Ferroelectrics*, **122,** 167.
[26] Nguyen, H. T., Rouillon, J. C., Cluzeau, P., Sigaud, G., Destrade, C., and Isaert, N., 1994, *Liq. Cryst.*, **17,** 571.
[27] Takezoe, H., Lee, J., Chandani, A. D. L., Gorecka, E., Ouchi, Y., Fukuda, A., Terashima, K., and Furukawa, K., 1991, *Ferroelectrics*, **114,** 187.
[28] Nishiyama, I., and Goodby, J. W., 1992, *J. mater. Chem.*, **2,** 1015.
[29] Booth, C. J., Dunmur, D. A., Goodby, J. W., Haley, J., and Toyne, K. J., 1996, *Liq. Cryst.*, **20,** 387.
[30] Tuffin, R. P., Goodby, J. W., Bennemann, D., Heppke, G., Lötszch, D., and Scherowsky, G., 1995, *Mol. Cryst. liq. Cryst.*, **260,** 51.
[31] Watanabe, J., and Hayashi, M., 1989, *Macromolecules*, **22,** 4083.
[32] Watanabe, J., and Kinoshita, S., 1992, *J. Phys. II Fr.*, **2,** 1237.
[33] Takanishi, Y., Takezoe, H., Fukuda, A., Komura, H., and Watanabe, J., 1992, *J. mater. Chem.*, **2,** 71.
[34] Fukui, M., Orihara, H., Yamada, Y., Yamamoto, N., and Ishibashi, Y., 1989, *Jpn. J. appl. Phys.*, **28,** L849.
[35] Naciri, J., Ratna, B. R., Baral-Tosh, S., Keller, P., and Shashidhar, R., 1995, *Macromolecules*, **28,** 5274.
[36] Apfel, M. A., Finkelmann, H., Janini, G. M., Laub, R. J., Luhmann, B. H., Price, A., Roberts, W. L., Shaw, T. J., and Smith, C. A., 1985, *Anal. Chem.*, **57,** 651.
[37] Li, J., Takezoe, H., and Fukuda, A., 1991, *Jpn. J. appl. Phys.*, **30,** 532.
[38] Goodby, J. W., Patel, J. S., and Chin, E., 1992, *J. mater. Chem.*, **2,** 197.
[39] Neundorf, M., Takanishi, Y., Fukuda, A., Saito, S., Murashiro, K., Inukai, T., and Demus, D., 1995, *J. mater. Chem.*, **5,** 2221.
[40] Miyasato, K., Abe, S., Takezoe, H., Fukuda, A., and Kuse, E., 1983, *Jpn. J. appl. Phys.*, **22,** L661.
[41] Mery, S., and Shashidhar, R., unpublished results.
[42] Goodby, J. W., Slaney, A. J., Booth, C. J., Nishiyama, I., Vuijk, J. D., Styring, P., and Toyne, K. J., 1994, *Mol. Cryst. liq. Cryst.*, **243,** 231.
[43] Suzuki, Y., Nonaka, O., Koide, Y., Okabe, N., Hagiwara, T., Kawamura, I., Yamamoto, N., Yamada, Y., and Kitazume, T., 1993, *Ferroelectrics*, **147,** 109.
[44] Kelly, S. M., 1993, *Liq. Cryst.*, **14,** 675 and references therein.

[45] Percec, V., and Pugh, C., 1989, in *Side Chain Liquid Crystal Polymers*, edited by C. B. McArdle (New York: Chapman and Hall).
[46] Ringsdorf, H., and Schneller, A., 1982, *Makromol. Chem. rapid Commun.*, **3,** 557.
[47] Dumon, M., Nguyen, H. T., Mauzac, M., Destrade, C., and Gasparoux, H., 1991, *Liq. Cryst.*, **10,** 475.
[48] Cooray, N. F., Kakimoto, M. A., Imai, Y., and Suzuki, Y., 1994, *Macromolecules*, **27,** 1592.
[49] Gray, G. W., Hawthorne, W. D., Lacey, D., White, M. S., and Semlyen, J. A., 1989, *Liq. Cryst.*, **6,** 503 and references therein.
[50] Richard, H., Mauzac, M., Sigaud, G., Achard, M. F., and Hardouin, F., 1991, *Liq. Cryst.*, **9,** 679.
[51] Matsuzaki, K., Kanai, T., Kawamura, T., Matsumoto, S., and Uryu, T., 1973, *J. Polym. Sci. Polym. Chem. Ed.*, **11,** 961.
[52] Frosini, V., Magagnini, P. L., and Newman, B. A., 1974, *J. Polym. Sci. Polym. Phys. Ed.*, **12,** 23.
[53] Newman, B. A., Frosini, V., and Magagnini, P. L., 1975, *J. Polym. Sci. Polym. Chem. Ed.*, **13,** 87.
[54] Frosini, V., Levita, G., Lupinacci, D., and Magagnini, P. L., 1981, *Mol. Cryst. liq. Cryst.*, **66,** 21.